19th Australasian Fluid Mechanics Conference
Melbourne, Australia
8-11 December 2014

Modelling Water Wave and Tethered Structure Interactions using 3D Smoothed Particle Hydrodynamics

D. F. Gunn[1], M. Rudman[1] and R. C. Z. Cohen[2]

[1]Department of Mechanical and Aerospace Engineering
Monash University, Clayton, Victoria 3800, Australia

[2]CSIRO Computational Informatics
Gate 5 Normanby Road, Clayton, Victoria 3168, Australia

Abstract

Knowledge of how a floating offshore structure will react to the rough conditions of the seas, particularly during storms, is critical to their safe and efficient design. This paper describes the first step in validating a Smoothed Particle Hydrodynamics model for analysing and predicting the response of floating structures to rough sea conditions. The validation cases considered are those of a tethered spherical buoy oscillating in the horizontal and vertical directions, and of the same buoy responding to incident wave trains. These cases are compared against experimental data obtained in a wave flume, with results showing the importance of adequate particle resolution.

Introduction

Small amplitude water waves have long been studied by scientists, and their interaction with simple structures can be accurately predicted by a wide range of mathematical approximations [3]. However, when the structures become more complex in design, analytical methods and mathematical approximations can no longer be used to solve the governing equations. Furthermore when the waves become large in amplitude, or more irregular, nonlinear effects become significant and a model describing the wave-structure interaction becomes increasingly difficult to obtain. Sophisticated numerical techniques are required when analysing these situations which occur frequently in the ocean.

One of the techniques that is capable of modelling the interactions between structures and fluids is Smoothed Particle Hydrodynamics (SPH) [1, 4, 6, 7, 8]. In this paper we utilise SPH to simulate the interaction between fluid and structures. The Lagrangian approach of SPH does not require a mesh to be used, which is advantageous when analysing fluid structure interaction on a free or constrained structure as the expensive remeshing stage is not required.

The SPH technique has previously been used to study the effect of fluid structure interactions, and a number of benchmark tests have been conducted previously. Doring et al. [2] tested the problem of water entry of a wedge, achieving good agreement between experimental and their 2D numerical results. Le Touzé et al. [5], and Rudman and Cleary [8] both conducted 3D SPH simulations of a large wave impacting a structure (a ship and an oil platform respectively), but Le Touzé et al.'s results over predicted the water heights, and Rudman and Cleary did not present a comparison with experiments. Cummins, Sylvester, and Cleary [1] presented a thorough benchmark case for a dam-break problem, measuring the impact of flood water on a fixed square column, achieving good agreement with experiments.

These studies however do not consider structures that are tethered to the ocean floor. Structures such as Tension Leg Platforms and offshore wind turbines are tethered to the ocean floor due to being placed in waters that are too deep to be fixed. In this paper we present two benchmark cases for such scenarios utilising a rising tethered sphere; oscillation in the vertical and horizontal directions, and the motion under the influence of an incident wave train. The results of the comparisons between simulations and experiments will help to determine what simulation parameters are critical to ensure simulation accuracy when modelling tethered structures..

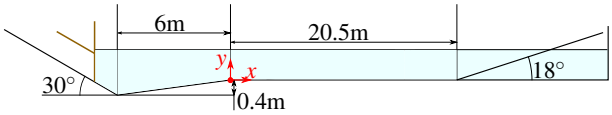

Figure 1. Wave tank schematic

Experimental Setup

The experiments were conducted in a 40 m long, 1 m wide wave tank at Monash University, a schematic of which can be seen in Figure 1. The tank contains a 20.5 m testing section that has a horizontal floor, a 6 m long development region, and an inclined beach at the end of the test section. A piston type wavemaker is located prior to the development region that moves on an incline of 30° to the horizontal. A wave absorbing beach is located at the end of the testing section, rising on an incline of 18°. The depth of the tank is measured in the testing section, and for this study is filled to a depth of 0.8 m.

The coordinate system was chosen with y-axis pointing upwards, the $y = 0$ plane corresponding to the floor of the test section, and the $z = 0$ plane corresponding to the mid-plane of the tank. The x-axis was defined in the lengthwise direction of the tank with $x = 0$ located at the start of the test section. The coordinate system can be seen in Figure 1 by the red arrows with the z coordinate pointing out of the page.

For each experiment a tethered spherical buoy is used to observe the fluid-structure interaction. The sphere is tethered by a cable, spring (stiffness $k = 30.88$ N/m), and pulley system as depicted by the schematic in Figure 2. The spherical buoy used has diameter of 0.203 m, mass of 1.7451 kg, and centre of mass located 27 mm vertically below the centre of the sphere (towards the cable attachment point). Relative to the drag of the buoy moving through the water, the pulley system provides insignificant damping.

The cable and spring initial lengths were set to ensure that at the rest position half the sphere is submerged. The location of the pulley system is such that the buoy centroid is located at $x = 1.15$ m. The pulley system is required to ensure that the coil spring used does not extend or contract within the water and cause the spring to be damped.

In each of the experiments the trajectory of the sphere was mea-

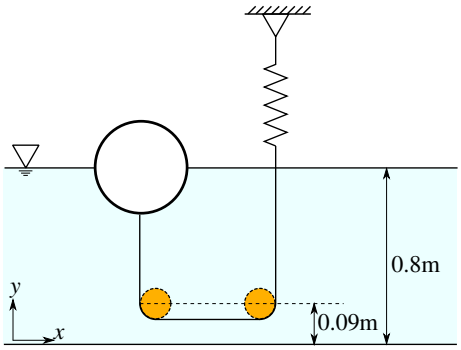

Figure 2. Experimental setup of the buoy at its equilibrium position.

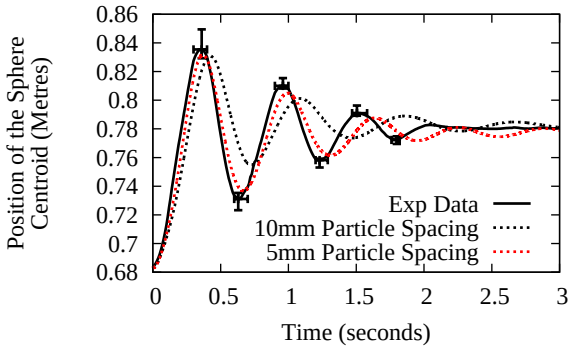

Figure 3. Sphere Centroid Trajectory for the Vertical Oscillation cases

sured using position tracking software developed at CSIRO. The software determines the 3D location of a visible landmark based on the location within the frame of view of at least two camera angles. Four cameras were used and placed around the buoy in the experiments, allowing the cameras to observe up to 11 landmarks on the surface of the buoy at any point in time. The 3D locations of these marks could then be used to determine the location of the sphere's centroid. The buoy is painted with an alternating black and white octant pattern, with the corners of the octants used as markers and three additional markers painted in each of the white octants.

SPH Solver

In this study the SPH implementation of Cummins, Sylvester, and Cleary [1] is used. For brevity, the reader is directed to their paper for a thorough discussion on the SPH method.

Oscillation Tests

The first benchmark case considered in this work is two tests of a tethered sphere oscillating in the vertical and horizontal directions respectively. These tests provide a simple first benchmark case as an entry point to the validation study, and also give insight into the natural frequency of the buoys motion in each direction. In order to reduce computational expense, only a short section of the wave tank is included in the simulations for each test. The vertical oscillation tests only modelled a 1 m length of the tank while the horizontal tests modelled a 2 m length of the tank. Shorter tank lengths were not considered as the truncated lengths would be shorter than the tank width or would not leave enough space for the buoy to oscillate.

For the vertical oscillation test, the buoy was pulled under the surface so it was completely submerged by 15 mm, and then released to return to the rest position. The vertical trajectory of the sphere centroid was measured, and the amplitude and period

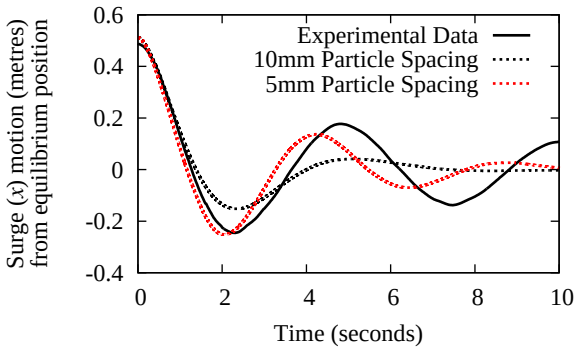

Figure 4. Buoy displacement in the x direction for the Horizontal Oscillation test

of oscillation were compared to simulations. Figure 3 shows a comparison between the experimental vertical trajectory (obtained from the mean of 7 experiments) and the trajectories observed in simulations with different resolutions. The test with 10 mm particle spacing achieves a good estimate of the amplitude of the first crest, however the amplitude thereafter and the period of oscillation are poor. Refining the particle spacing to 5 mm results in a trajectory that is much closer to the experimental results. However the amplitude of the troughs and crests beyond the first crest are still under estimated, and the period of oscillation is too long.

In the horizontal oscillation test, the buoy was displaced by 0.5 m in the x direction only and released to return to the rest position. The trajectories in each direction were measured, and a comparison between experiments and simulations was performed. Figure 4 shows the horizontal trajectory of the buoy in both the experiments and a simulation with particle spacing of 10 mm. The period of oscillation in the horizontal direction appears to be in good agreement between the experiments and simulation, however the amplitude of motion is severely damped in the simulation. Again only a small amount of data has been obtained for the 5 mm resolution case, however the data collected thus far is in good agreement with the experimental data.

Finally, by measuring the time between peaks of the experimental trajectories in Figures 3 and 4, an estimation of the natural frequency of oscillation can be determined for each direction. These give natural frequencies of 1.67 Hz for the vertical motion, and 0.18 Hz for the horizontal motion.

Wave Train Tests

The interaction between the buoy and an incident wave train is the second benchmark considered in this work. Wave trains with periods of 1 and 3 seconds are considered, with two different amplitudes. The smaller amplitude tests are denoted as Experiments 1A and 3A, while the tests with larger amplitudes are denoted as Experiments 1B and 3B. Table 1 summarises the mean wave amplitudes used in each of the experiments.

The motion recorded in the experiments and simulations is then non-dimensionalised by the following expressions:

$$x^* = \frac{(x - x_e)kd}{a} \tag{1}$$

$$y^* = \frac{(y - y_e)}{a} \tag{2}$$

$$t^* = \frac{t - t_0}{T} \tag{3}$$

where d is the depth, a is the mean wave amplitude, T is the

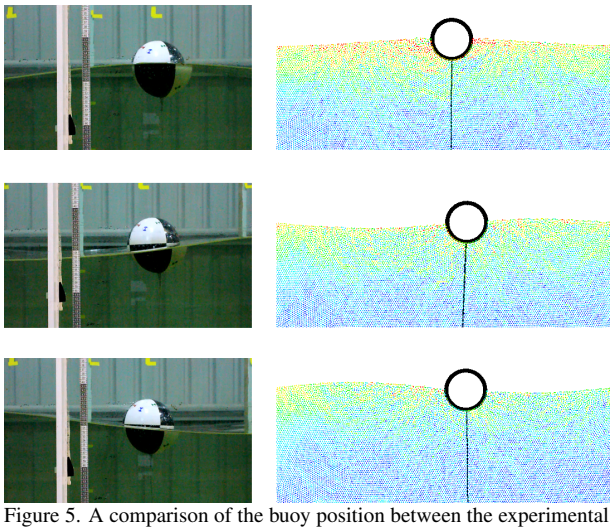

Figure 5. A comparison of the buoy position between the experimental (left) and simulated (right) buoys in a 1 second period wave train. The top image corresponds to $t^* = 0$, the second to $t^* = 0.3$, and the final to $t^* = 0.7$. In the simulations the fluid particles are coloured by speed.

wave period, k is the wave number, (x_e, y_e) is the equilibrium position of the buoy, and t_0 is the time at which the buoy is atop the first full sized crest. There is very little motion in the z direction so the z motion of the buoy is not considered.

Two SPH simulations with mean particle spacings of 10 mm were then performed, one creating a 1 second period wave train and the other creating a 3 second period wave train using a fluid control routine based on the shallow wave equations. The wave amplitudes of the simulations were 4.5 cm and 6.0 cm respectively, chosen as approximate midpoints of the experimental wave amplitudes.

Figure 5 shows a number of side views of the buoy in a 1 second period wave train, both experimental (case 1A) and simulated. The position of the buoy relative to the wave in each frame are in good agreement between the experiments and simulations.

For the 1 second case, Figure 6 the experimental heave motions of the buoy are in good agreement after $t^* = 0$, and the simulated peaks are also in good agreement. Figure 7 shows a large amplitude modulation of the trajectory is observed in the surge, the amplitude of which appears to depend on the amplitude of the wave train. The same modulation is also observed in the simulation, however the amplitude is much smaller. At this resolution heavy damping was observed in the horizontal oscillation simulation test and this is likely to also reduce the amplitude of the modulation. Figures 8 and 9 show the frequency spectra of the motion in the surge and heave motions respectively. The dashed vertical lines in each indicate the natural frequency in the respective direction of oscillation, as determined in the Oscillation Tests. As expected the frequency spectra contain clear peaks at 1 Hz, the frequency of the wave train, however in the surge frequency spectra, peaks can be observed at the natural frequency, indicating that the frequency of the modulation is at the natural frequency.

Experiment	Wave Amplitude (cm)
1A	3.2
1B	5.8
3A	4.7
3B	7.1

Table 1. Mean wave amplitudes used in the Wave Train tests

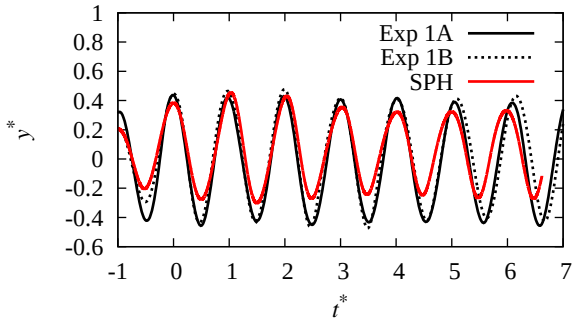

Figure 6. Heave motion of the buoy in response to a 1 second period wave train

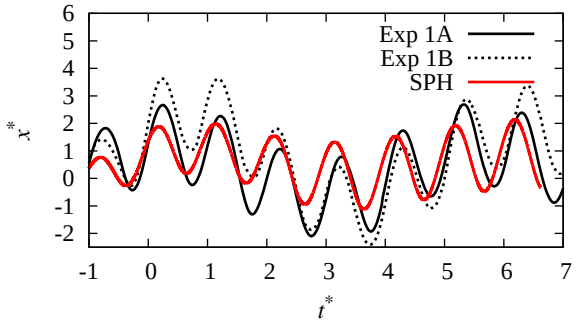

Figure 7. Surge motion of the buoy in response to a 1 second period wave train

In the 3 second period case, the crests of the buoy heave motion (Figure 10) are in very good agreement with each other, however the troughs have some disagreement. The disparity at the bottom of the troughs is due to the cable that tethers the buoy going into slack for the 3B and simulation cases but not in the 3A case. Since the cable can only provide a tension force, the troughs in 3B and the simulation have no tethering force, while there is some tethering force in 3A. The experimental results for the surge motion (Figure 11) are in good agreement, however the simulation results are inaccurate at the troughs and the surge motion is out of phase with the experiments. Similar to the 1 second case, this could be due to over damping predictions in SPH at such a coarse resolution.

In both of the Oscillation tests the resolution was observed to be an influential parameter in determining the accuracy of the simulation. In these cases a refined resolution can be expected to return numerical predictions that more closely match the experimental results.

Conclusion

In this paper the interactions between a tethered buoy and both static water and wave trains were studied numerically and compared to experimental results. The simulation technique, SPH, achieved good results in predicting the motion of the buoy under the various effects. However the resolution of the study has a significant impact on the accuracy of the simulation. Using too coarse a resolution caused the period of oscillations in the vertical direction to be overpredicted, and the surge motion becomes significantly damped. When a finer resolution is used there is closer agreement between the experiment and simulation results.

This paper has shown us that with adequate resolution, SPH becomes a powerful tool in predicting the consequences of a

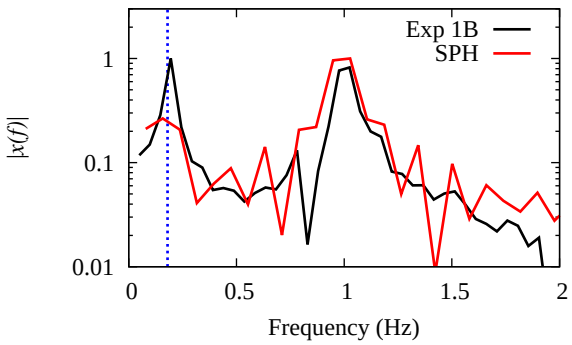

Figure 8. Frequency spectra for the buoy motion in the surge direction under the influence of a 1 second period wave train. The vertical dashed line indicates the natural frequency of 0.18 Hz

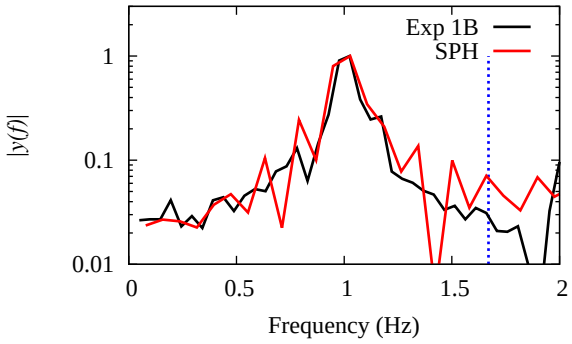

Figure 9. Frequency spectra for the buoy motion in the heave direction under the influence of a 1 second period wave train. The vertical dashed line indicates the natural frequency of 1.67 Hz

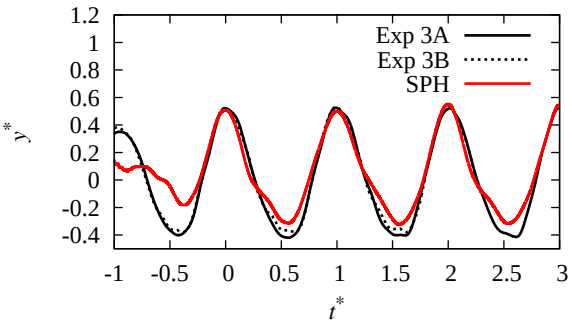

Figure 10. Heave motion of the buoy in response to a 3 second period wave train

fluid and tethered structure interaction. Future continuation of this work will explore the impact of a breaking wave over the buoy in a bid to show that SPH can be used to model rough sea conditions effectively.

Acknowledgements

The authors would like to thank CSIRO HPC for providing the cluster that the simulations were performed on, Jon Hinwood of Monash University for providing access to the wave tank and assisting in the experiments, and the Monash University Mechanical Workshop for building and providing the equipment used in the experiments.

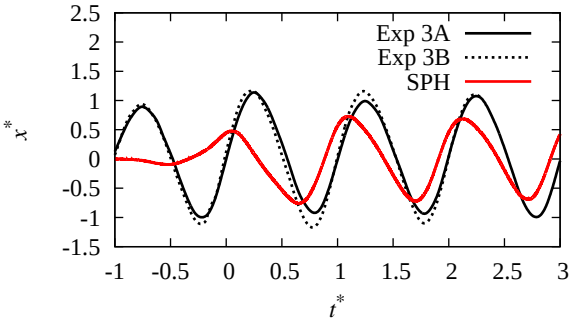

Figure 11. Surge motion of the buoy in response to a 3 second period wave train

References

[1] Cummins, S. J., Silvester, T. B. and Cleary, P. W., Three-dimensional wave impact on a rigid structure using smoothed particle hydrodynamics, *International journal for numerical methods in fluids*, **68**, 2012, 1471–1496.

[2] Doring, M., Oger, G., Alessandrini, B. and Ferrant, P., SPH Simulations of Floating Bodies in Waves, in *Proceedings of OMAE04, 23rd International Conference on Offshore Mechanics and Arctic Engineering*, 2004, Vancouver, British Columbia, Canada, June 20-25.

[3] Faltinsen, O. M., Wave Loads on Offshore Structures, *Annu. Rev. Fluid Mech.*, **22**, 1990, 35–56.

[4] Gingold, R. A. and Monaghan, J. J., Smoothed particle hydrodynamics: theory and application to non-spherical stars, *Mon. Not. R. Astr. Soc.*, **181**, 1977, 375–389.

[5] Le Touzé, D., Marsh, A., Oger, G., Guilcher, P. M., Khaddaj-Mallat, C., Alessandrini, B. and Ferrant, P., SPH simulation of green water and ship flooding scenarios, *Journal of Hydrodynamics, Ser. B*, **22**, 2010, 231–236.

[6] Monaghan, J. J., Smoothed Particle Hydrodynamics, *Annu. Rev. Astron. Astrophys.*, **30**, 1992, 543–574.

[7] Monaghan, J. J., Simulating Free Surface Flows with SPH, *Journal of Computational Physics*, **110**, 1994, 399–406.

[8] Rudman, M. and Cleary, P. W., Rogue wave impact on a tension leg platform: The effect of wave incidence angle and mooring line tension, *Ocean Engineering*, **61**, 2013, 123–138.